Normal Development

2

Kamaldine Oudjhane

Contents

Abstract

The development of the musculoskeletal system encompasses the embryonic period, fetal development, and the lengthy postnatal period of growth and maturation. This chapter emphasizes the growth of the infant, child, and adolescent but briefly reviews key points of prenatal development. Understanding cartilage maturation is key to understanding bone development, as well as imaging of normal development and pathology. After reviewing the process of physeal bone deposition, the chapter presents MRI appearance of cartilage, focusing on the primary and secondary physes. It discusses normal developmental physiologic periostitis of infancy. The chapter concludes by discussing several different systems for establishing skeletal maturity and reviewing for which ages each is most applicable.

The development of the musculoskeletal system encompasses the embryonic period, fetal development, and the lengthy postnatal period of growth and maturation. This chapter emphasizes the development of the infant, child, and adolescent but briefly reviews key points of the prenatal period. Understanding cartilage maturation is key to understanding bone development, as well as imaging of normal development and pathology. After reviewing the process of physeal bone deposition, the chapter reviews the magnetic

K. Oudjhane, MD, MSc
Diagnostic Imaging Department,
The Hospital for Sick Children, University of Toronto,
555 University Avenue, Toronto, ON M5G 1X8, Canada
e-mail: kamaldine.oudjhane@sickkids.ca

R. Stein-Wexler et al. (eds.), *Pediatric Orthopedic Imaging*,
DOI 10.1007/978-3-642-45381-6_2, © Springer-Verlag Berlin Heidelberg 2015

resonance imaging (MRI) appearance of cartilage, focusing on the primary and secondary physes. It discusses normal developmental physiologic periostitis of infancy. The chapter concludes by discussing several different systems for establishing skeletal maturity and reviewing for which ages each is most applicable. Bone marrow maturation is presented in Chap. 25, which addresses both normal and pathologic bone marrow.

1 General Cartilage and Bone Development

1.1 Embryonic and Fetal Development

Musculoskeletal development starts during the embryonic period, or the first 8 weeks after conception. Following formation of the trilaminar embryonic disk during the first 2 weeks, induction starts the process of tissue specialization and subsequent organogenesis [1]. Primordial organogenesis occurs during the first 4 weeks, and major defects in limb development can occur at this time. Key landmarks of skeletal development in the embryo and fetus are summarized below.

Embryonic Development:

- Week 3: The embryonic disk develops, with individualization of somites and the neural tube.
- Week 4: The somites differentiate into three segments—dermatome (skin), myotome (muscle), and sclerotome (cartilage and bone). The embryo is very sensitive to major defects in limb development during this period. During week 4, the limb buds originate as elevations of the fetal unsegmented mesenchyme. The upper limb buds appear shortly before those of the lower limb, and the upper extremity continues to develop more quickly than the lower until about age 2 years.
- Week 5: Mesenchyme condenses in the limbs, and the hand plate is formed.
- Week 6: Mesenchyme chondrifies. Digits individualize.
- Week 7: Notching occurs between the digits, and the upper and lower limbs rotate in opposite directions.
- Week 8: The embryo is recognizably human.

Fetal Development:

The fetal stage is characterized by rapid changes in body proportions, with the following highlights:

- Week 12: Bone development spreads beyond the clavicle, the first bone to ossify. The relatively short lower limbs grow rapidly.
- Week 14: Clefting of mesenchyme results in the formation of synovial joints. This is followed by chondrification and cavitation.
- Week 16: The development of the neuromuscular system allows for spontaneous limb activity. Hematopoiesis, which had started in the yolk sac and then liver, begins in bone as the marrow space develops [2].
- Week 20: Growth and remodeling of body proportions continue, and the fetus develops an infant-like form.

Much of the skeleton forms by endochondral ossification. Mesenchyme condensation occurs first, forming cartilage, which is then transformed to bone [3]. This occurs at the skull base, long and tubular bones, clavicles, and vertebral column. Primary ossification centers develop within the diaphyses of the long bones, in the vertebrae, in a few epiphyses, and in some of the smaller bones before birth. Their formation requires changes in the perichondrium: degeneration of hypertrophic cells and increased vascularity form an ossified core at the cartilage-bone interface. Most of the epiphyses and small bones ossify after birth. The flat bones—such as the pelvis, scapula, skull, and facial bones—form by intramembranous ossification, which occurs without a cartilaginous precursor.

1.2 Infancy and Childhood

Fetal woven bone is flexible and has a high collagen content; it is replaced by lamellar bone during infancy. Most of the smaller bones develop primary ossification centers during infancy.

During childhood, the long bones undergo further growth, with tremendous increase in length as well as thickness. Secondary ossification centers develop at the ends of the long bones. Longitudinal growth of long bones depends principally on the primary physis, adjacent to the metaphysis. The secondary physis, which surrounds the epiphysis, results in the more spherical configuration at the ends of the long bones. Transverse growth at the diaphysis occurs by intramembranous bone formation at the periosteum, which consists of an outer fibrous layer and an inner layer composed of osteoprogenitor cells.

Physis

The physeal cartilage includes three well-defined histologic zones: resting, proliferative, and hypertrophic. Its composition is the same whether at the primary physis (abutting the metaphyses) or at the secondary physis (surrounding the secondary ossification centers), but the secondary physis is thinner. The resting zone is closest to the metaphysis or secondary ossification center and contains an abundant, disorganized matrix of chondrocytes. These are the germinator stem cells of the physis. The proliferative zone has longitudinal columns of rapidly dividing chondrocytes responsible for increased bone length. It is rich in glycogen; rapid extracellular matrix turnover takes place here. Chondrocyte proliferation and differentiation are highly regulated by secreted growth factors that activate chondrocyte-specific transcription factors [4]. The hypertrophic zone abuts the cartilage and includes a segment where chondrocytes mature, a segment of degeneration (with disintegration of mucopolysaccharides and declining blood supply), and a zone of provisional calcification. The zone of provisional calcification is closest to the metaphysis and marks the transition from bone to cartilage; this is the weakest part of the growth plate.

The periphery of the metaphysis, adjacent to the physis, is a very vascular site of active bone formation and remodeling. The perichondrial ring of LaCroix and the groove of Ranvier constitute the periphysis, a fibro-chondro-osseous structure that encircles the growth plate and the most recently developed portion of the metaphysis [5]. The periphysis and bone formed by the gradual transverse growth of the physis make up the metaphyseal collar in the young child; this may protrude from the metaphyseal contour and must be differentiated from a corner metaphyseal fracture (see Chap. 18).

The vascular system plays a major role in growth plate physiology [6]. Three major pathways supply the physis: the epiphyseal arteries of the secondary ossification center reach the proliferative segment, the diaphysial nutrient arteries provide a capillary network to the metaphyseal-physeal junction, and the perichondrial arteries supply the periphysis. Bone remodeling occurs by funnelization, with bone resorption and deposition; longitudinal growth and shaping at the epiphysis, metaphysis, and diaphysis result. The acrophyses, including the epiphyses, apophyses, carpals, tarsals, and growth plates at nonphyseal ends of the small tubular bones, make up the growth plates of the secondary ossification centers [7].

Cartilage

The ends of the long bones are composed of hyaline cartilage. Although all hyaline cartilage consists of chondrocytes and water within a matrix of collagen and glycosaminoglycans, the architecture and the exact composition vary. Epiphyseal cartilage, physeal cartilage (whether at the primary physis or at the secondary physis that surrounds the epiphyseal ossification center), and articular cartilage therefore appear different on some MRI sequences.

Articular cartilage is hypocellular and avascular; it consists predominantly of a collagen and proteoglycan matrix. Physeal cartilage is very cellular, especially the hypertrophic zone; it is vascular until age 18 months and then becomes avascular. Epiphyseal cartilage is very vascular while the ossification center is developing [8, 9]. The articular cartilage functions to transmit and buffer force, whereas the epiphyseal and physeal cartilage contribute to growth. With maturation, the appearance of epiphyseal and physeal cartilage changes.

2 Cartilage Imaging

MRI differentiates between joint fluid and articular cartilage; it can also differentiate between epiphyseal, physeal, and articular cartilage because of their different compositions [10]. At histological examination, hyaline cartilage of the epiphysis demonstrates chondrocytes within a matrix rich in water, collagen, glycoproteins, and glycosaminoglycans. The water is bound to collagen fibers, and only a small fraction is free. The orientation of the collagen fibers is uniform in the physeal and epiphyseal cartilage. However, in the articular cartilage—where it is less tightly bound to water—its pattern varies depending on location. The superficial collagen fibers parallel the articular surface, whereas those in the deep zone are perpendicular to the surface; those in the intermediate zone have a more random arrangement [11]. Some MRI sequences demonstrate subtle differences in signal intensity, corresponding to these different zones.

A variety of sequences have been developed to image cartilage, and others allow molecular and functional imaging. As a general rule, cartilage imaging requires at least a 1.5 tesla (T) magnet. Cartilage is, in general, isointense to muscle on T1-weighted (T1-W) imaging (Fig. 2.1) and relatively hypointense on fluid-sensitive sequences [12]. T1-W and intermediate-weighted proton density (PD) sequences are superb for showing morphology of ligaments and menisci. However, these sequences offer little information about architecture of the hyaline cartilage of the epiphysis, as its signal intensity is uniform on these sequences [13] (Fig. 2.2). Hyaline cartilage also shows uniform signal intensity (high to intermediate) on gradient echo (GRE) sequences. Decreasing the flip angle (to 15–20°) on these sequences increases T2 weighting and thus helps differentiate hypointense cartilage from more hyperintense joint fluid [8].

Fluid-sensitive sequences, such as short tau inversion recovery (STIR) and T2-weighted (T2-W) (especially fat-suppressed (FS) sequences), characterize cartilage architecture better than T1-W sequences (Fig. 2.3). On these fluid-sensitive sequences, signal intensity of physeal and articular cartilage is higher than that of epiphyseal cartilage, probably due to increased cellularity and free water in the growth plate cartilage compared with epiphyseal cartilage. Because the physeal cartilage has longer T2 values, increasing the echo time (TE) enhances the contrast between epiphyseal and physeal cartilage. 3D dual-echo steady-state imaging (3D-DESS) is also useful for imaging cartilage, improving the accuracy of cartilage thickness assessment (Fig. 2.4). Regardless of the sequence employed, adequate spatial resolution is essential for satisfactory imaging of cartilage.

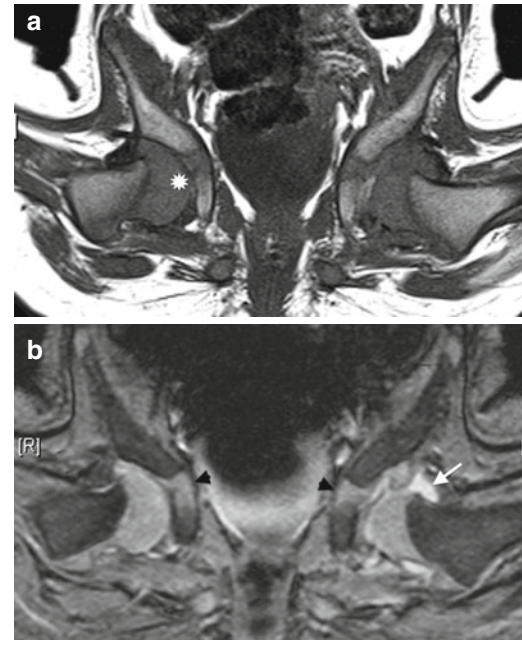

Fig. 2.1 Homogeneous appearance of femoral head cartilage in a 6-month-old. (**a**) Coronal T1-weighted (T1-W) image shows the epiphysis (*asterisk*) is of homogeneous intermediate signal intensity. (**b**) Coronal gradient echo (*GRE*), fast field echo (*FFE*) image shows moderately hyperintense cartilage signal, along with a small amount of very hyperintense joint fluid (*white arrow*) on the left. Note cartilaginous triradiate cartilage (*black arrowheads*), which has similar signal intensity to the femoral head

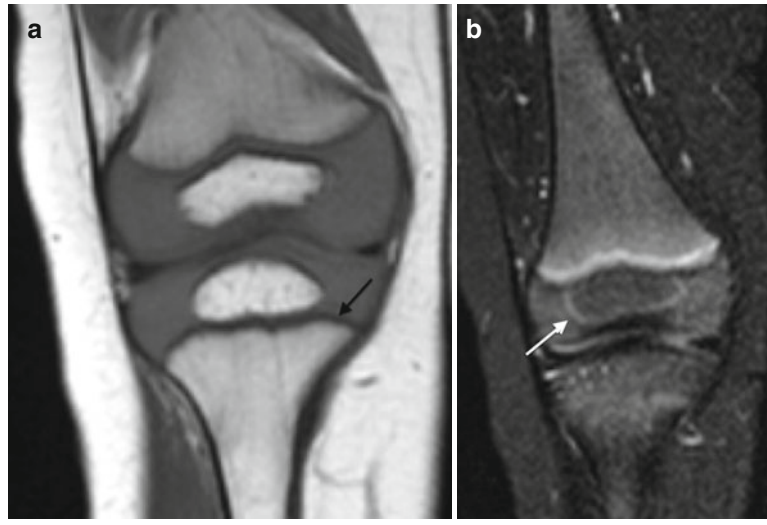

Fig. 2.2 Normal infant knee. (**a**) Coronal T1-W image shows the growth plate and epiphyseal cartilage have homogeneous intermediate signal. The zone of provisional calcification (*ZPC*) is hypointense (*arrow*) adjacent to the hyperintense metaphysis. (**b**) Coronal STIR image shows the primary physis is hyperintense, compared to the intermediate signal epiphyseal cartilage. The secondary physis, surrounding the epiphyseal ossification center, is also hyperintense (*arrow*) but much thinner than the primary physis (Courtesy of Marilyn Ranson)

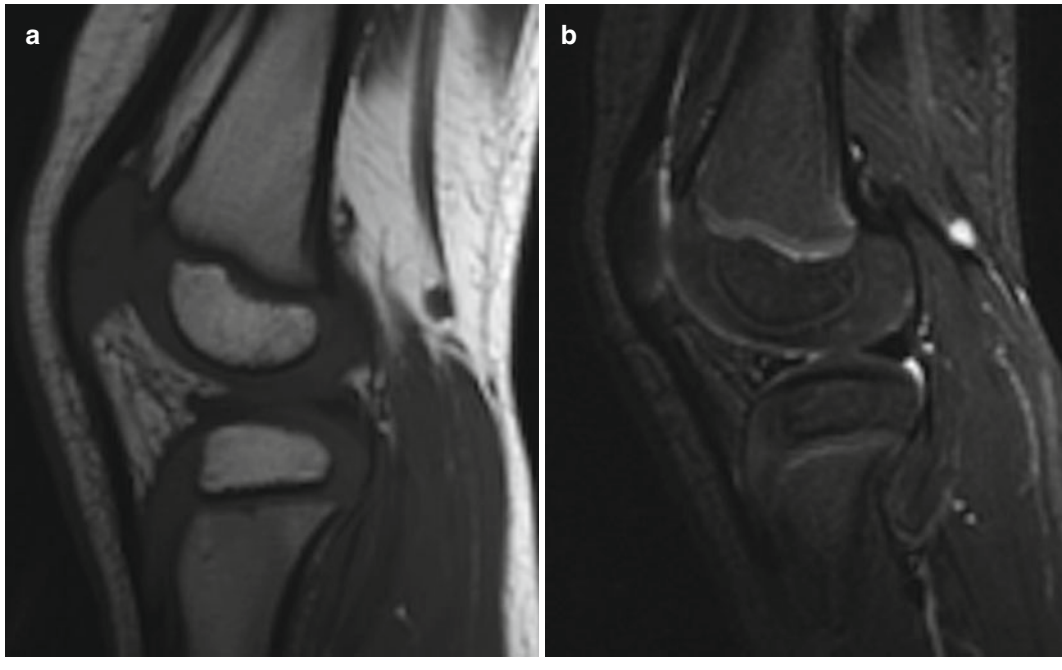

Fig. 2.3 Epiphyseal cartilage in a 4-year-old boy. (**a**) Sagittal T1-W image shows uniformly isointense cartilage (compared to muscle). (**b**) Sagittal inversion recovery (*IR*) image shows isointense signal intensity (compared to muscle) in the cartilage surrounding the ossified epiphysis and hyperintense physeal cartilage (Courtesy of Rebecca Stein-Wexler)

Fig. 2.4 Epiphyseal cartilage contrasted against joint fluid on sagittal 3D double-echo steady-state (*3D-DESS*) image of the knee in a 13-year-old boy. The epiphyseal and articular hyaline cartilage is slightly less bright than the joint fluid

With development, the cartilage changes in several ways. Epiphyseal cartilage evolves from its infantile appearance of uniform intermediate signal on T1-W images and moderate hyperintensity on fluid-sensitive sequences [12]. As ossification begins, fluid-sensitive sequences demonstrate patchy, heterogeneous (more hyperintense) areas, likely due to increased free water. These are most evident at the posterior distal femoral condyle and the trochlea of the distal humerus, but are also seen elsewhere [14] (Fig. 2.5). Cartilage at weight-bearing areas (e.g., the acetabulum and the distal and proximal femur) develops decreased T2 signal as the child begins walking, probably as water is displaced from cartilage [15] (Fig. 2.6).

The physeal cartilage at both the primary physis and at the peri-epiphyseal secondary physis has specific architecture that yields a trilaminar appearance on MRI (Figs. 2.7 and 2.8). The portion that abuts the metaphysis, the zone of provisional calcification, is densely mineralized and thus markedly hypointense on all sequences. The remainder of the physeal cartilage, like the articular cartilage, resembles unossified epiphyseal cartilage on T1-W images and is predominantly hypointense. However, on fluid-sensitive sequences, this portion of the physis (the germinal and proliferative zones as well as part of the hypertrophic zone) is brighter than epiphyseal cartilage, yielding the second identifiable layer [13]. The

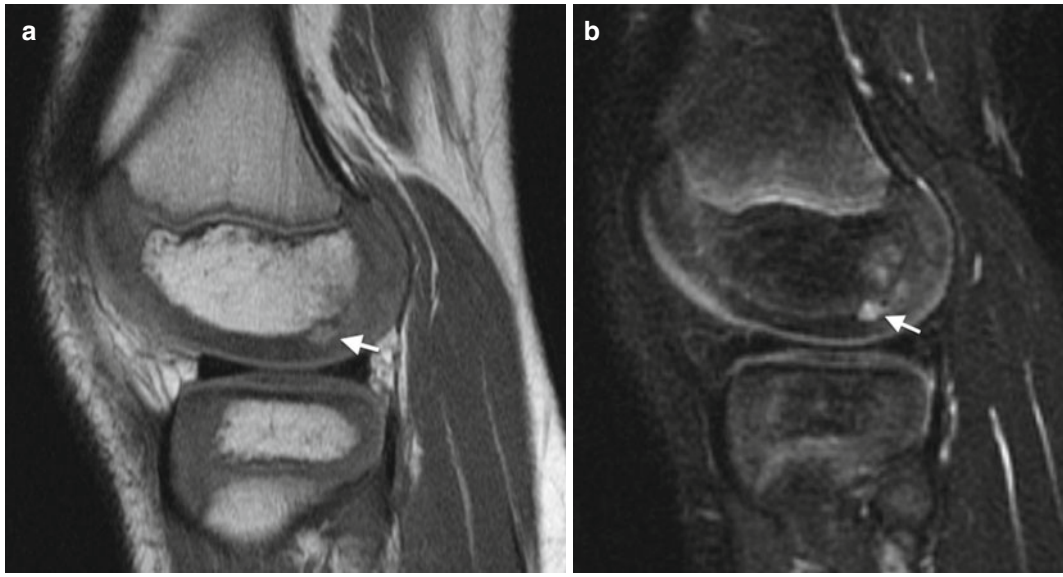

Fig. 2.5 Normal hyperintense pre-ossification centers within epiphyseal cartilage. Sagittal PD (**a**) and fast spin echo (*FSE*) T2-W FS (**b**) show pre-ossification (*arrows*) (Courtesy of Marilyn Ranson)

Fig. 2.6 *Morphological* changes in cartilage with maturation in a 6-year-old boy. Sagittal T2-weighted (*T2-W*) image with fat-suppressed (*FS*) knee image shows the weight-bearing epiphyseal cartilage of the femoral condyle has a relatively low signal, likely related to displacement of water from cartilage (*arrow*). A focus of increased signal in the posterior epiphyseal cartilage of femoral cartilage (*curved arrow*) likely represents the hyperintense fluid condensation that can be seen prior to the onset of ossification. In addition, the hyperintense articular cartilage (*arrowhead*) contrasts against the more intermediate signal of the epiphyseal cartilage

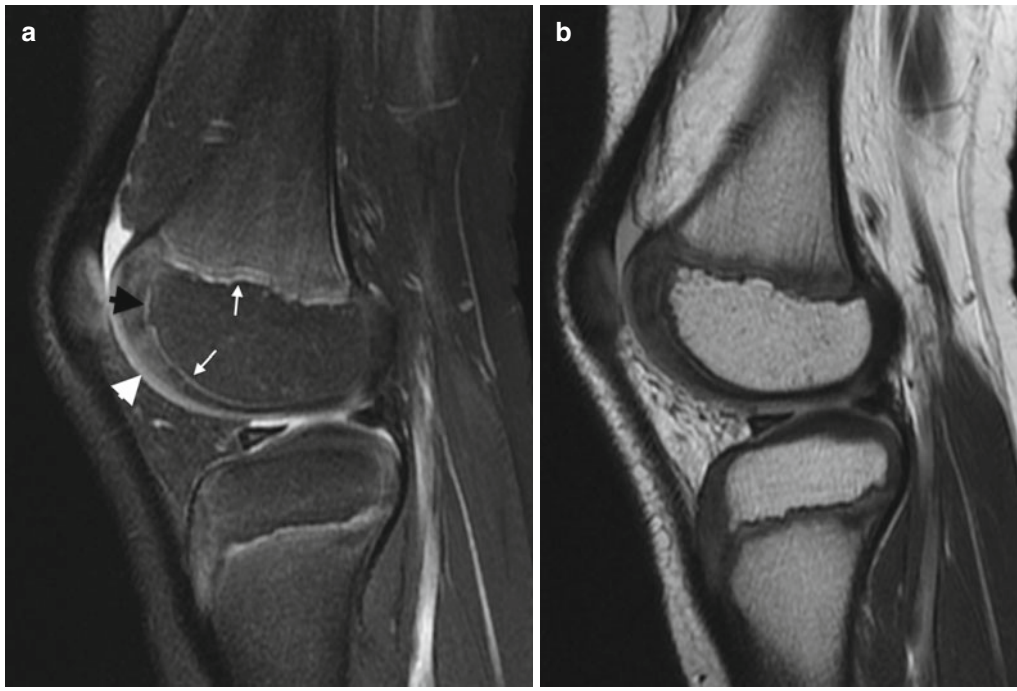

Fig. 2.7 Normal appearance of physeal, epiphyseal, and articular cartilage in a 7-year-old boy. (**a**) Sagittal PD FS image shows hypointense ZPC (*white arrows*), moderately hyperintense physeal cartilage (*black arrowhead*), and moderately hyperintense articular cartilage (*white arrowhead*). The ossified portion of the epiphysis is hypointense, and the remainder of the epiphyseal cartilage is heterogeneously hyperintense. (**b**) Sagittal PD image also demonstrates the various cartilage regions (Courtesy of Rebecca Stein-Wexler)

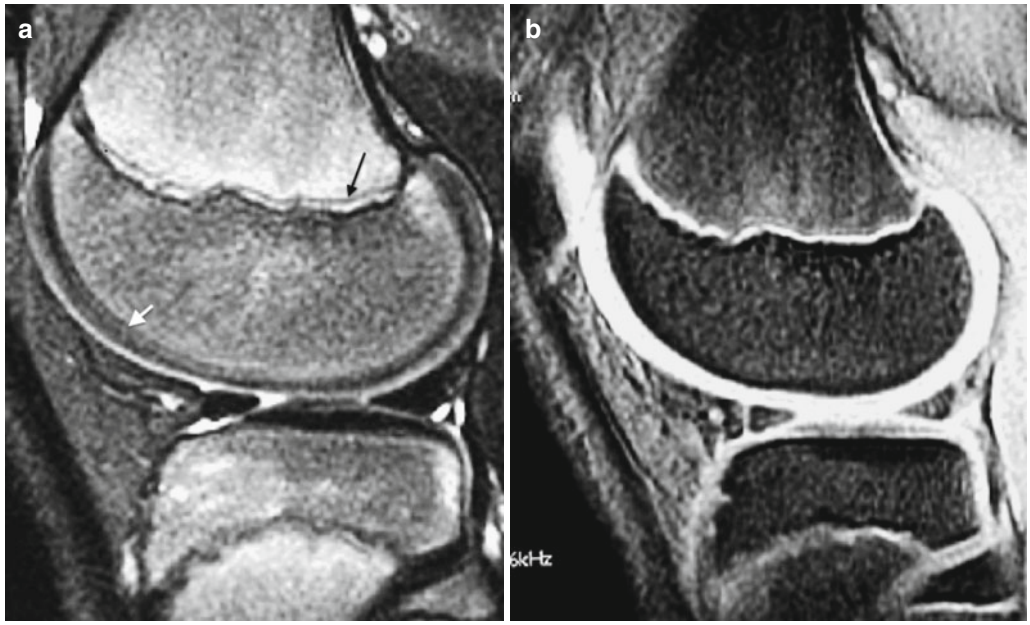

Fig. 2.8 Normal appearance of cartilage in an adolescent knee. (**a**) Sagittal FSE T2-W FS image shows trilaminar appearance with hyperintense metaphyseal spongiosa, hypointense ZPC (*black arrow*), and hyperintense physis. The epiphyseal cartilage (*white arrow*) has lower signal than articular cartilage. (**b**) Sagittal multiplanar T1-W GRE image shows uniformly bright cartilage signal (Courtesy of Marilyn Ranson)

physis that surrounds the ossification center in the epiphysis, the secondary physis, has similar architecture and signal intensity but is thinner.

Epiphyseal ossification begins in a single ossification center (as at the distal femur), in two centers (as at the proximal humerus), or in several centers (as at the trochlea of the distal humerus). The contour may be irregular. Normal signal intensity at MRI helps differentiate multiple ossification centers from fragmentation of a single center. If there is a single focus of ossification, ossification begins in the center of the epiphysis. Initially spherical, as endochondral bone forms, the shape changes to hemispheric, with the flat portion adjacent to the primary physis [16]. Although epiphyseal marrow is initially, like the adjacent metaphysis, hematopoietic, within a few months it becomes uniformly fatty (see Chap. 25).

Development of carpal bones, tarsal bones, and apophyses is similar to that of epiphyses. They therefore also demonstrate conversion to fatty marrow much sooner than do the metaphyses of long bones.

In very young children, the primary physis is flat and smooth, but with growth its contour begins to undulate [8]. It should still have uniform thickness, unless it has been damaged (e.g., after fracture or as a result of chronic stress in athletes). The physis thins with maturation and eventually fuses and disappears, sometimes leaving a very thin hypointense linear scar. Physeal fusion usually begins in the center of the physis and spreads to the periphery. The exception to this is at the distal tibia, where the anteromedial physis fuses first (at Kump's bump) and fusion progresses posterolaterally.

Epiphyseal cartilage is initially perfused by vessels within cartilage canals; these gradually become smaller and less numerous. Vascularization is most readily appreciated after administration of intravenous gadolinium, on fat-suppressed T1-W images. The vascular channels of the cartilaginous epiphysis exhibit linear and punctate areas of high signal intensity (the punctate areas are vascular channels viewed on end). Before the age of 18 months, some channels cross from metaphysis to epiphysis, and vascular canals are arrayed parallel to each other and to the long axis of the bone. As the secondary ossification center develops, the orientation of the vascular channels changes, so

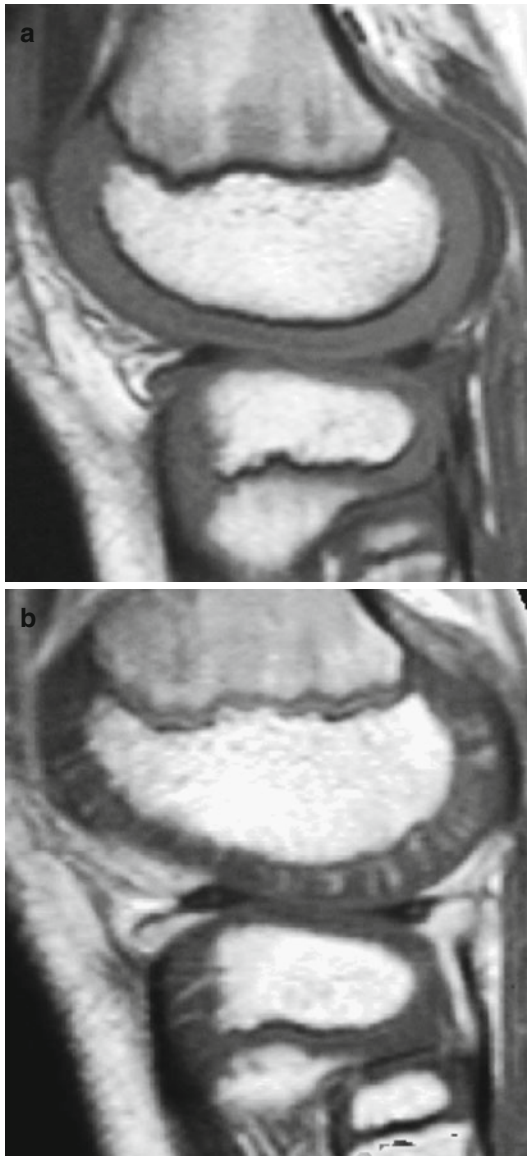

Fig. 2.9 Radiating array of epiphyseal vessels in a young child. (**a**) Sagittal T1-W MRI shows homogeneous intermediate signal of the epiphyseal and articular cartilage. (**b**) With GRE, radiating vascular channels are evident. The physes also enhance (Courtesy of Marilyn Ranson)

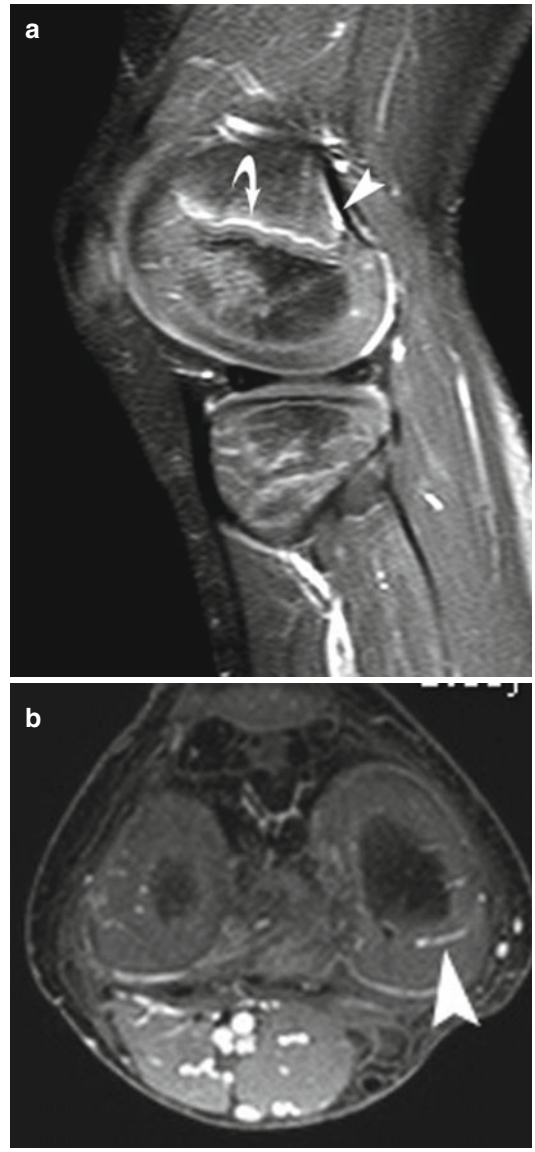

Fig. 2.10 Normal appearance of epiphyseal vasculature in a 6-year-old. Gadolinium-enhanced T1-W fast field echo (*FFE*) fat-suppressed (*FS*) MRI shows, on sagittal view (**a**), enhancement of the primary spongiosa of new metaphyseal bone (*curved arrow*). There is also enhancement of the subperiosteal fibrovascular tissue that forms the posterior metaphyseal stripe (*arrowhead*). (**b**) Axial image shows typical spoke-wheel pattern of vascular channels in the epiphyseal cartilage (*arrowhead*)

that they are arrayed in a spoke-like fashion around the ossifying epiphysis [9] (Fig. 2.9). During most of childhood, metaphyseal and epiphyseal blood flow are separate, with important consequences for trauma as well as spread of infection and tumor.

Gadolinium-enhanced sequences allow definition of the fibrovascular cuff and the primary spongiosa of new bone formation; it also delineates the posterior metaphyseal stripe, which is a subperiosteal band of fibrovascular tissue that contributes to growth (Fig. 2.10). In older patients, specialized MRI techniques such as

delayed gadolinium-enhanced MRI (dGEMRIC) and T2 mapping allow visualization of the four unique zones of articular cartilage: superficial or tangential, middle or transitional, deep or radial, and calcified [11]. In higher field-strength magnets, 3D isotropic techniques can be applied to cartilage imaging [17].

3 Physiologic Periostitis of Infancy (Box 2.1)

Box 2.1: Physiologic Periostitis of Infancy

1–4 months old (residual findings occasionally seen to 6 months old)
Bilateral in 40–70 %
Frequency: tibia > femur > humerus > ulna > radius
<2 mm thick
Diaphysis

Physiologic periostitis of infancy is a normal physiologic process wherein new bone forms rapidly by intramembranous ossification along the periosteum of the diaphysis of long bones. This can be identified in one third to one half of infants between 1 and 4 months of age. The residual finding of subperiosteal bone blending into cortex can be seen occasionally as late as 6 months of age [18]. Periosteal new bone results from the rapid growth that is characteristic of early infancy, combined with the fact that in children the periosteum is relatively thick and loosely attached. It generally involves both the upper and lower extremities [19] and is bilateral in 40–75 % (especially at the femur) [18]. The tibia is affected most often, followed by the femur, humerus, ulna, and radius.

The periosteal new bone initially appears as a faint amorphous line paralleling the diaphysis of the long bone, separated from the cortex by a thin lucent line. Not necessarily concentric, it may be seen on only one projection (Fig. 2.11). As the child grows, the layer of new bone thickens and becomes denser, briefly resembling a double cortex. It is gradually absorbed into the cortex, where it contributes to bone width.

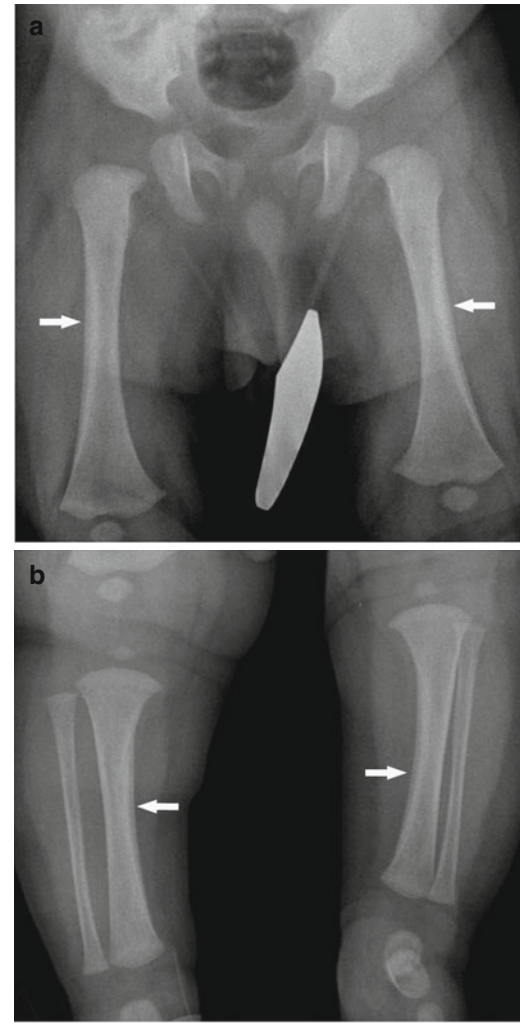

Fig. 2.11 Physiologic periostitis of infancy in a 2-month-old boy. Frontal views show bilateral lamellar bone formation (*arrows*) along the lateral diaphyseal cortex of both femurs (**a**) and along the medial diaphyseal cortex of both tibias (**b**)

Physiologic periostitis is differentiated from pathologic periostitis by its thinness (less than 2 mm), by the fact that it spares the metaphysis, and by the typical age at presentation, 1–4 months [18]. It should not be confused with osteomyelitis, infantile cortical hyperostosis, trauma, vitamin A intoxication, leukemia, or metastatic neuroblastoma.

4 Skeletal Maturation

Assessment of skeletal maturity is important in several clinical scenarios: in the setting of a suspected hormonal abnormality (e.g., precocious puberty), to help predict adult height (especially important in children with short stature), and to determine appropriate timing of surgery for scoliosis or for leg-length discrepancy. Radiologic assessment of skeletal maturity relies on evaluation of mineralization, maturation, and morphology of the ossification centers and comparison of these observations to standards.

Many methods of bone age assessment have been developed, but they are plagued by questions about accuracy, statistical validity, and interobserver variability [20, 21]. Furthermore, there are marked sexual, racial, familial, and environmental influences on bone development. For example, the sequence of ossification in the hand and wrist varies such that the triquetrum may ossify in any order ranging from the 3rd to the 24th of the 28 centers [22]. Some standards are based on a specific population group and do not necessarily apply to others [21, 23]. Girls differ from boys, not only in their advanced maturity but also in the order of ossification, and black infants are more skeletally mature than white infants. Therefore it is important to consider the standards as approximations and to always include a range of two standard deviations in estimating bone age. Computer-assisted measurement appears to increase statistical power [24].

Skeletal maturity in different parts of the body can be discordant, and this affects timing of surgical intervention. Discrepancy may be striking in the hand and wrist, where carpal maturation may lag behind or precede phalangeal maturation by several years. This can be syndromic or associated with disease but is more often inconsequential. However, up to 40 % of patients demonstrate a 1-year difference in physeal fusion between the distal forearm and the leg, and physeal closure in the hand may precede or follow physeal closure in the tibia by up to 2 years. This has important implications for timing of surgery. More important than the precise stage of skeletal maturity of the hand, elbow, or iliac crest is the state of maturation in the bone (or bones) being considered for potential intervention.

Skeletal maturity may be assessed by several methods, depending on patient age. In premature infants and during the prenatal period, the presence of specific ossification centers correlates with patient age. During the first year of life, the method of Sontag can be used (see below) [25]. During much of childhood, skeletal age determination is based on a PA view of the left hand, according to the methods of Greulich and Pyle, Tanner, Gilsanz and Ratib, and others [26–28]. However, during the pubertal growth spurt, these methods become less accurate, and skeletal age can be determined by the configuration of the olecranon apophysis [29] and then, later, by the status of the iliac crest apophysis [30].

Before birth and in premature infants, age can be assessed by determining whether ossification has begun in key centers. A few important prenatal ossification standards follow:

- Dental buds at 20–21 weeks, +/– 2 weeks
- Calcaneus at 24 weeks
- Talus at 28 weeks
- Distal femur epiphysis at 36 weeks
- Proximal tibial epiphysis at 38 weeks
- Proximal humeral epiphysis at 40–41 weeks

In addition, throughout childhood, multiple ossification centers provide rough landmarks for skeletal maturity [20] (see Table 2.1).

In infants less than 1 year old, skeletal maturation can be determined by the Sontag method [25]. This method counts secondary ossification centers in half of the skeleton, based on a radiograph of the entire left upper extremity (including the shoulder to the distal epiphyses of the fingers) and a second radiograph of most of the left lower extremity (from the mid-femur to the distal epiphyses). All secondary ossification centers except the talus and calcaneus are counted, including the coracoid and other centers at the shoulder. The total number of ossification centers in the hemiskeleton is compared with normal values for children up to age 1.5 years (see Table 2.2).

From age 1 year through adolescence, evaluation of the hand is generally performed, though interpretation is plagued by questions of statistical accuracy. Specificity is lower and standard deviations greater during the adolescent growth spurt, and other bones may be evaluated at this age, as discussed below. The Greulich and Pyle

Table 2.1 Selected ossification centers, 50th percentile age at appearance

	50th percentile age at appearance	
	Boys	Girls
1. Infancy		
Capitate	3 m	2 m
Hamate	4 m	2 m
Capitellum of humerus	4 m	3 m
Capital femoral epiphysis	4 m	4 m
Cuneiform 3	6 m	3 m
Humerus greater tuberosity	10 m	6 m
2. Early childhood		
Cuneiform 1	2 y, 2 m	1 y, 5 m
Cuneiform 2	2 y, 8 m	1 y, 10 m
Navicular of the foot	3 y	1 y, 11 m
Fibula proximal epiphysis	3 y, 6 m	2 y, 7 m
Patella	4 y	2 y, 6 m
3. Childhood		
Radius head	5 y, 3 m	3 y, 10 m
Medial epicondyle of humerus	6 y, 3 m	3 y, 5 m
Calcaneal apophysis	7 y, 7 m	5 y, 4 m
Olecranon of ulna	9 y, 8 m	8 y
Lateral epicondyle of humerus	11 y, 3 m	9 y, 3 m
4. Adolescence		
Tibial tubercle	11 y, 10 m	10 y, 3 m
Adductor sesamoid of thumb	12 y, 9 m	10 y, 9 m
Acromion	13 y, 9 m	11 y, 11 m
Iliac crest	14 y	12 y, 9 m
Coracoid apophysis	14 y, 4 m	12 y, 3 m
Ischial tuberosity	15 y, 3 m	13 y, 11 m

Adapted from Ref. [20]
y year, *m* month

Table 2.2 Age based on presence of hemi-skeleton ossification centers in the infant

	Number of centers in boys		Number of centers in girls	
Age (months)	Mean	1 S.D.	Mean	1 S.D.
1	4.1	1.4	4.6	1.8
3	6.6	1.9	7.8	2.2
6	9.6	1.9	11.4	2.5
9	11.9	2.6	15.4	4.9
12	14	4.0	22.4	6.9
18	19.3	6.6	34.1	8.4

Adapted from Ref. [25]

method compares the appearance, growth, modeling, and fusion of the metacarpal and phalangeal epiphyses as well as the carpal centers to standard hand radiographs [26]. Table 2.3 is based on the atlas of Greulich and Pyle and summarizes changes during the early adolescent period after ossification of the adductor sesamoid. Tanner's method assigns a score to the carpal bones (except the pisiform) and to the epiphyses of the distal ulna, distal radius, and metacarpals and phalanges of the first, third, and fifth rays. These are summed to establish an individual's skeletal maturity scale and do not directly refer to patient age [27]. A digitally formatted atlas of the hand, developed by Gilsanz and Ratib, includes a large range of sample populations and is statistically more accurate [28].

Assessment of skeletal maturity around puberty is very important, because the success of some surgical interventions depends on the precise timing of when they are performed. Puberty can be divided into two phases: acceleration and deceleration [31]. The pubertal growth spurt (on average, age 11–13 for girls and 13–15 for boys) is considered accelerational. Growth is rapid—and the rate of growth increases—during this time. The subsequent 3 years (on average, age 13–16 for girls and 15–18 for boys) are considered decelerational, as growth gradually ceases. Different methods of bone age assessment have varying utility during these periods.

The Sauvegrain method, which evaluates the ossification centers of the elbow, assesses maturation during growth acceleration but is static during deceleration, when all physes have fused. The Risser method, in contrast, which evaluates the iliac crest apophysis, is static during acceleration but useful during deceleration. The method of Greulich and Pyle is fairly accurate before the pubertal growth spurt but relatively imprecise during both the accelerational and decelerational growth phases.

During the acceleration phase of skeletal maturation, the ossification centers of the elbow change dramatically, from being predominantly cartilaginous to being fully fused. Indeed, they change enough in the course of 6 months to allow determination of skeletal maturity on a semiannual basis, which helps fine-tune surgical planning. The Sauvegrain method analyzes the size and shape of the lateral condyle and epicondyle, trochlea, olecranon, and radial head apophyses on

Table 2.3 Estimation of skeletal age in adolescence

	Skeletal age in boys		Skeletal age in girls	
Bone	Age (years)	1 S.D. (months)	Age (years)	1 S.D. (months)
Small adductor sesamoid	13	10.4	11	11.9
Large adductor sesamoid	13.5–14	10.7	12	10.2
DP 1, fusion almost complete DP 2–5, partial fusion in male	15	11.3	13	10.6
DP, all fused PP, partial fusion	15.5	–	13.5	–
DP, all fused MP, partial fusion PP, fusion almost complete	16	12.9	14	11.3
DP, MP, PP, all fused	17	13	15	9.2
Radius, partial fusion	18	–	16	7.3

Adapted from Ref. [26]
DP distal phalanx epiphysis, *MP* middle phalanx epiphysis, *PP* proximal phalanx epiphysis

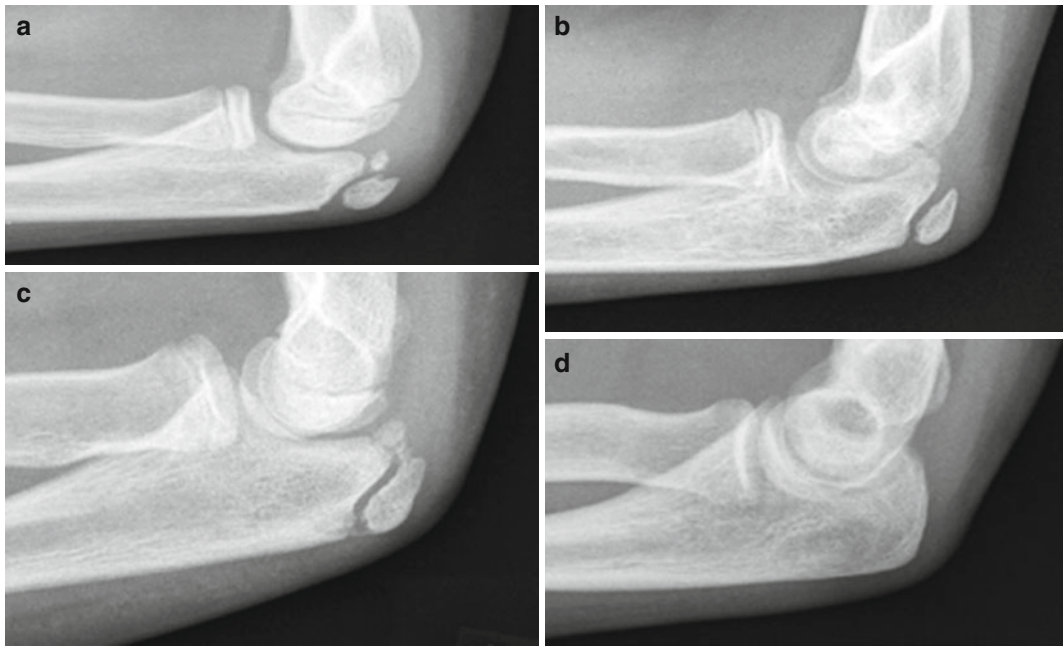

Fig. 2.12 Maturation of the olecranon. According to the simplified Sauvegrain method, the configuration of the olecranon ossification changes from (**a**) two ossific centers, to (**b**) a single half-moon-shaped center, to (**c**) a rectangular center, to (**d**) a center that has completely fused to the ulna

frontal and lateral views to provide a relatively accurate means of assessing skeletal maturity [29]. It is also possible to employ a simplified Sauvegrain method, which focuses on the appearance of the olecranon apophysis viewed on a lateral radiograph [31]. The olecranon changes from having two ossification centers initially (at age 11 in girls, 13 in boys) to resembling a half-moon 6 months later and to appearing more rectangular after another 6 months. It then begins fusion (age 12.5 in girls, 14.5 in boys) and 6 months later is fully fused to the ulna [31] (Fig. 2.12) (Table 2.4).

The configuration of the iliac crest apophysis begins to change 6 months after the elbow physes close, so Risser staging is applied to the decelerational growth phase. The apophysis at the iliac crest ossifies in a predictable manner—initially lateral, with progressive ossification of the more

Table 2.4 Skeletal maturation indices in the second decade

Girls	Boys	Risser scale	Olecranon	Fusion of epiphyses
11 y	13 y	0	2 centers	
11.5 y	13.5 y		Half-moon	
12 y	14 y		Rectangle	
12.5 y	14.5 y		Begins fusion	
13 y	15 y		Fusion complete	
13 y, 8 m	14 y, 7 m	1		Distal phalanx epiphyses [2–5]
14 y, 6 m	15 y, 7 m	2		Proximal phalanx epiphyses Greater trochanter apophysis
15 y, 2 m	16 y, 2 m	3		Distal phalanx epiphyses [1, 2]
16 y, 2 m	17 y	4		Distal ulnar epiphysis
18 y, 1 m	18 y, 6 m	5		Distal radial epiphysis

Adapted from Refs. [26, 30–32]
y year, *m* month

central portions as the more peripheral portions undergo fusion. At Risser 0, the apophysis has not yet ossified, and at Risser 5 it is fully formed and fused. The intermediate stages divide the iliac crest into quartiles (see Chap. 3 for additional discussion of the Risser method).

Maturation of the hand, elbow, and iliac crest should correlate (Table 2.4). The olecranon matures during early puberty (11–13 years in girls, 13–15 years in boys), when the iliac crest registers as Risser 0 (non-ossified apophysis). Risser 1 occurs at the same time as fusion of the distal phalanges in the hand. At Risser 2, the greater trochanter fuses to the femur, and the metacarpal epiphyses fuse. Risser 3 occurs at the same time as closure of the epiphyses of the middle phalanges. At Risser 4, the distal ulna fuses. Finally, Risser 5 is a lengthy period during which the distal radius epiphysis gradually fuses to the radius.

Skeletal maturity can also be used to estimate adult stature. The Bayley and Pinneau tables [33] are easy to use, but a more accurate system devised by Roche and colleagues integrates variables such as present height, weight, skeletal age, and parental stature [34].

References

1. Hall BK. The embryonic development of bone. Am Sci. 1988;76(2):174–81.
2. Babyn PS, Ranson M, McCarville ME. Normal bone marrow: signal characteristics and fatty conversion. Magn Reson Imaging Clin N Am. 1998;6(3):473–95. PubMed PMID: 9654581.
3. Dietz FR, Morcuende JA. Embryology and development of the musculoskeletal system. In: Morrissy RT, Weinstein SL, editors. Lovell and Winter's pediatric orthopedics: sixth edition. 6th ed. Philadelphia: Lippincott Williams & Wilkins; 2005. p. 1–33.
4. Wuelling M, Vortkamp A. Chondrocyte proliferation and differentiation. Endocr Dev. 2011;21:1–11. PubMed PMID: 21865749.
5. Oestreich AE, Ahmad BS. The periphysis and its effect on the metaphysis: I. Definition and normal radiographic pattern. Skeletal Radiol. 1992;21(5):283–6. PubMed PMID: 1502578.
6. Gray H, Standring S, Ellis H, Berkovitz BKB. Gray's anatomy: the anatomical basis of clinical practice. 39th ed. Edinburgh/New York: Elsevier Churchill Livingstone; 2005. xx, 1627 pp.
7. Oestreich AE. The acrophysis: a unifying concept for enchondral bone growth and its disorders. I. Normal growth. Skeletal Radiol. 2003;32(3):121–7. PubMed PMID: 12605274.
8. Jaramillo D, Laor T. Pediatric musculoskeletal MRI: basic principles to optimize success. Pediatr Radiol. 2008;38(4):379–91. PubMed PMID: 18046547.
9. Barnewolt CE, Shapiro F, Jaramillo D. Normal gadolinium-enhanced MR images of the developing appendicular skeleton: Part I. Cartilaginous epiphysis and physis. AJR Am J Roentgenol. 1997;169(1):183–9. PubMed PMID: 9207522.
10. Khanna PC, Thapa MM. The growing skeleton: MR imaging appearances of developing cartilage. Magn Reson Imaging Clin N Am. 2009;17(3):411–21, v. PubMed PMID: 19524193.
11. Potter HG, Foo LF. Magnetic resonance imaging of articular cartilage: trauma, degeneration, and repair. Am J Sports Med. 2006;34(4):661–77. PubMed PMID: 16365371.
12. Laor T, Jaramillo D. MR imaging insights into skeletal maturation: what is normal? Radiology. 2009;250(1):28–38. PubMed PMID: 19092089.
13. Jaramillo D, Connolly SA, Mulkern RV, Shapiro F. Developing epiphysis: MR imaging characteristics and histologic correlation in the newborn lamb.

Radiology. 1998;207(3):637–45. PubMed PMID: 9609885.
14. Chapman VM, Nimkin K, Jaramillo D. The preossification center: normal CT and MRI findings in the trochlea. Skeletal Radiol. 2004;33(12):725–7. PubMed PMID: 15322770.
15. Varich LJ, Laor T, Jaramillo D. Normal maturation of the distal femoral epiphyseal cartilage: age-related changes at MR imaging. Radiology. 2000;214(3):705–9. PubMed PMID: 10715034.
16. Rivas R, Shapiro F. Structural stages in the development of the long bones and epiphyses: a study in the New Zealand white rabbit. J Bone Joint Surg Am. 2002;84-A(1):85–100. PubMed PMID: 11792784.
17. Naraghi A, White LM. Three-dimensional MRI of the musculoskeletal system. AJR Am J Roentgenol. 2012;199(3):W283–93. PubMed PMID: 22915419.
18. Kwon DS, Spevak MR, Fletcher K, Kleinman PK. Physiologic subperiosteal new bone formation: prevalence, distribution, and thickness in neonates and infants. AJR Am J Roentgenol. 2002;179(4):985–8. PubMed PMID: 12239052.
19. Shopfner CE. Periosteal bone growth in normal infants. A preliminary report. Am J Roentgenol Radium Ther Nucl Med. 1966;97(1):154–63. PubMed PMID: 5938033.
20. Graham CB. Assessment of bone maturation–methods and pitfalls. Radiol Clin North Am. 1972;10(2):185–202. PubMed PMID: 4339776.
21. Ontell FK, Ivanovic M, Ablin DS, Barlow TW. Bone age in children of diverse ethnicity. AJR Am J Roentgenol. 1996;167(6):1395–8. PubMed PMID: 8956565.
22. Garn SM, Rohmann CG, Silverman FN. Radiographic standards for postnatal ossification and tooth calcification. Med Radiogr Photogr. 1967;43(2):45–66. PubMed PMID: 6056078.
23. Gilsanz V, Skaggs DL, Kovanlikaya A, Sayre J, Loro ML, Kaufman F, et al. Differential effect of race on the axial and appendicular skeletons of children. J Clin Endocrinol Metab. 1998;83(5):1420–7. PubMed PMID: 9589632.
24. Gross GW, Boone JM, Bishop DM. Pediatric skeletal age: determination with neural networks. Radiology. 1995;195(3):689–95. PubMed PMID: 7753995.
25. Sontag LWS D, Anderson M. Rate of appearance of ossification centers from birth to the age of five years. Am J Dis Child. 1939;58:949–56.
26. Greulich WW, Pyle SI. Radiographic atlas of skeletal development of the hand and wrist. 2nd ed. Stanford: Stanford University Press; 1959. xvi, 256 pp.
27. Tanner JM. Assessment of skeletal maturity and prediction of adult height (TW2 method). London/New York: Academic; 1975. vii, 99 pp.
28. Gilsanz V, Ratib O. Hand bone age: a digital atlas of skeletal maturity. 2nd ed. New York: Springer; 2012.
29. Sauvegrain J, Nahum H, Bronstein H. Study of bone maturation of the elbow. Ann Radiol. 1962;5:542–50. PubMed PMID: 13986863.
30. Risser JC. The Iliac apophysis; an invaluable sign in the management of scoliosis. Clin Orthop. 1958;11:111–9. PubMed PMID: 13561591.
31. Dimeglio A, Charles YP, Daures JP, de Rosa V, Kabore B. Accuracy of the Sauvegrain method in determining skeletal age during puberty. J Bone Joint Surg Am. 2005;87(8):1689–96. PubMed PMID: 16085606.
32. Scoles PV, Salvagno R, Villalba K, Riew D. Relationship of iliac crest maturation to skeletal and chronologic age. J Pediatr Orthop. 1988;8(6):639–44. PubMed PMID: 3192691.
33. Bayley N, Pinneau SR. Tables for predicting adult height from skeletal age: revised for use with the Greulich-Pyle hand standards. J Pediatr. 1952; 40(4):423–41. PubMed PMID: 14918032.
34. Roche AF, Wainer H, Thissen D. Predicting adult stature for individuals. Monogr Paediatr. 1975;3:1–114. PubMed PMID: 1109427.

http://www.springer.com/978-3-642-45380-9

Pediatric Orthopedic Imaging
Stein-Wexler, R.; Wootton-Gorges, S.L.; Ozonoff, M.B. (Eds.)
2015, XXIV, 971 p. 1033 illus., 38 illus. in color.,
Hardcover
ISBN: 978-3-642-45380-9